Article

Analysis of Initiation Angle for Fracture Propagation Considering Stress Interference

Xia Xiao [1] and Cong Xiao [2],*

[1]   Department of City Construction, Wenhua College, Wuhan 430074, China; xclmjtud@126.com
[2]   Faculty of Applied Mathematics, Delft University of Technology, 2628CD Delft, the Netherlands
*   Correspondence: c.xiao@tudelft.nl; Tel.: +31-068-229-1075

check for updates

Abstract: Stress interference of multiplied fractures has significant influences on the propagation behavior of hydraulic fractures in roads, bridges, clay formations, and other forms of engineering. This paper establishes a crossing criterion and initiation angle model with comprehensive consideration of remote stress, stress intensity near the tip of fracture, and stress interference of multiplied fractures. Compared with the existing crossing criterion and initiation angle model, the ability to cross natural fractures decreases. Furthermore, the secondary initiation angle decreases with consideration of multiplied fracture propagation. The length of hydraulic fractures and natural fractures has little influence on the secondary initiation angle. With the increase in fracture space, the stress interference between fractures decreases, and as a result, the initiation angle begins to increase and then decrease. Differing from the propagation behavior of single fracture, the initiation angle basically does not vary with the increasing of net pressure under the high intersection angle between hydraulic fractures and natural fractures. Under a low intersection angle condition, the bigger the net pressure is, the smaller the initiation angle is. These results have great significance when analyzing the propagation behavior of multiplied fractures in real-world applications.

Keywords: stress interference; fracture propagation; crossing criterion; initiation angle

1. Introduction

It has been widely acknowledged that formation cracks have become an essential part of the security of engineering design in roads, bridges, formations, and other objects. Clay formations often contain cracks which have drastic influences on the propagation behavior of the induced fractures. It has been widely acknowledged that the interaction between induced fractures and natural cracks leads to complex topologies of crack systems. The interaction depends on rock stresses, mechanical properties, the orientation of the natural cracks, and operational engineering conditions including invaded fluid properties, loading rate, and magnitude. On the one hand, the induced cracks will remain planar when the induced cracks and natural cracks cross though each other directly. On the other hand, if the induced fractures are captured by the natural cracks, and then propagate along the natural crack, a fracture network with complex topology will be produced. Hence, accurate determination of the crossing behavior between induced fractures and natural cracks is a central task for the engineers on the condition of particular roads and bridges, including stress distribution, rock mechanical properties, and loading rate, because these conditions significantly control the topology of the produced fracture system [1–4].

In the process of fracture propagation, natural fractures and hydraulic fractures produce crossing behavior and result in a complex network of hydraulic fractures. On the basis of trail experiments, Daneshy et al. [5] and Blanton et al. [6], among others, concluded that three kinds of cross behaviors generally exist between natural fractures and hydraulic fractures: directly-penetrated natural fractures, fracture initiation and extension after the natural fracture partly opens, full opening of the natural

fracture, and fracture initiation and extension at the end of the fracture. They also found that the difference in crustal stress, the angle between natural cracks and hydraulic cracks, and rock strength all play significant roles in the behavior of cross extension and fracture initiation direction between hydraulic fractures and natural fractures. Both domestic and international researchers have studied the theory of crack and propagation behavior, and proposed the mechanic condition criterion of fracture initiation. Palaniswamy et al. put forward the energy release rate criterion [7], Erdogan et al. came up with the maximum circumferential stress criterion [8], Sih et al. put forward the strain energy density factor theory on the foundation of the maximum circumferential stress criterion [9], and Gu et al. analyzed the effect of re-fracturing initiation angle for the non-orthogonal natural fracture [10]. Based on the maximum circumferential stress criterion, Cheng et al. derived the calculation model of the fracture initiation angle after the full opening of natural fractures [11]. Combining with the strain energy density factor theory, Shao et al. built the calculation model of fracture initiation angle [12]. However, all of the above criteria are based on a single hydraulic fracture extension. The stress interference induced by the surrounding fractures has significant influence on the multiplied fracture propagation behavior. On the basis of the boundary element theory, Crouch et al. proposed the Displacement Discontinuity Method (DDM) and gave the analytical solution of the stress distribution around the two-dimensional fractures with an infinite fracture height [13]. By adding a modification factor, Olson et al. subsequently extended the DDM to three-dimensional fractures with finite fracture heights, to enable them to match actual situations [14].

Based on the existing research works in the literature, this paper built a new initiation angle model with the consideration of stress interference effects. By analyzing multiplied fracture propagation behaviors, the effects of fracture length, fracture distance, the relative position and length of natural cracks, and fluid invasion stress within the hydraulic cracks were investigated systematically. In addition, some comparisons with the existing calculation model of fracture initiation angle were also conducted. This study can provide theoretical guidance for real applications.

2. Analysis of Mechanical Condition

Network fracturing technology contains sequential multi-stage hydraulic fracturing and simultaneous multi-stage hydraulic fracturing. Hydraulic fractures are stimulated individually and sequentially for the former (Figure 1a), while hydraulic fractures are produced simultaneously for the latter (Figure 1b). As seen in Figure 1, an x–y coordination system can be established based on the orientation of the maximum principal stress (σ_H), and minimum principal stress (σ_h). Some other assumptions are described in the following text.
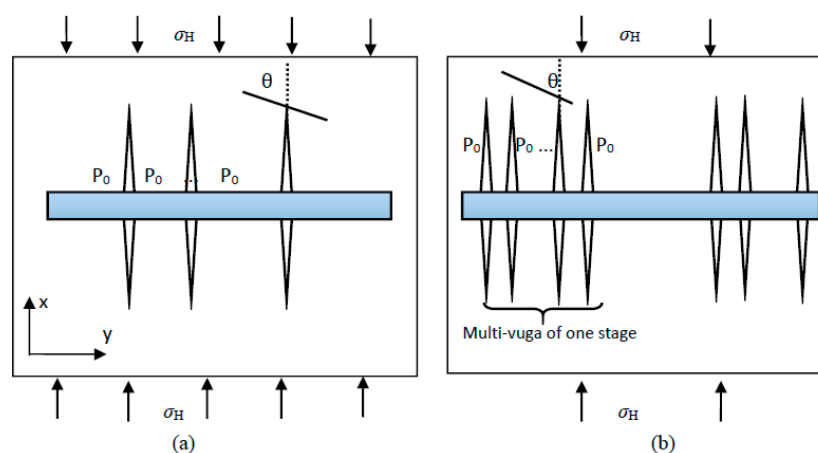

Figure 1. Illustration of network fracturing in clay formation: (**a**) multi-stage fracturing (**b**) multi-cluster fracturing. In this paper, two-dimensional planar fractures of finite height are considered. The black thin line represent the natural fracture, while the triangles denote the hydraulic fractures.

A hydraulic fracture initiates with the wellbore and is parallel to the maximum principal stress (σ_H), while normal to the minimum principal stress (σ_h), and the hydraulic fracture and natural fracture are vertical in profile.

Ignoring the pressure damage inside the horizontal wellbore, the number of hydraulic fractures for the former (Figure 1a) is equal to *N*, the number of hydraulic fractures for the latter (seen from Figure 1b) is equal to *M*, and the net pumping pressure is approximately equal to P_0.

One natural fracture exists around the vicinity of hydraulic fracture and crosses with one hydraulic fracture. The intersection angle between natural cracks and hydraulic crack is θ.

In the operation of fracture propagation for clay formation, the propagation of the fracture is mainly impacted by three kinds of mechanical conditions: in situ horizontal stress (σ_H and σ_h), the intensive stress at the tip of hydraulic cracks, and the induced interference stress among neighboring hydraulic cracks. Therefore, the total stress at the site of intersection between the natural cracks and the hydraulic fracture is the vector superposition of those three stresses.

2.1. Intensive Stress at the Tip of the Hydraulic Fracture

In terms of those two network fracturing technologies, Figure 2 illustrates one special hydraulic fracture and its forehead natural fracture which will intersect with this hydraulic fracture. Therefore, the stress surrounding the tip of this hydraulic fracture induced by the stress intensity is presented as follows [10]:

$$\begin{cases} \sigma_{tip,x} = \frac{K_I}{\sqrt{2\pi r}} \cos\frac{\alpha}{2}\left(1 - \sin\frac{\alpha}{2}\sin\frac{3\alpha}{2}\right) \\ \sigma_{tip,y} = \frac{K_I}{\sqrt{2\pi r}} \cos\frac{\alpha}{2}\left(1 + \sin\frac{\alpha}{2}\sin\frac{3\alpha}{2}\right) \\ \tau_{tip,xy} = \frac{K_I}{\sqrt{2\pi r}} \sin\frac{\alpha}{2}\cos\frac{\alpha}{2}\cos\frac{3\alpha}{2} \end{cases}. \tag{1}$$
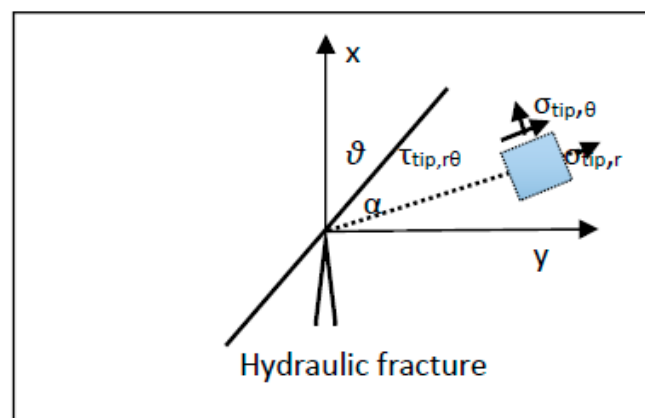

Figure 2. The illustration of stress distribution at the tip of the hydraulic fracture. The thin, black line represent the natural fracture. The dotted line denotes one random scenario of the natural fracture which is used for the analysis of stress distribution.

Based on some relevant theories proposed by Cheng et al. [11], the maximum stress criterion should be employed to identify whether the rock will be destroyed. The crack mechanics assume that the materials will be yielded within the transitional zone at the tip of hydraulic fractures. According to the micro-mechanical strain mechanisms, the stress inside the transitional zone should not exceed the stress at the position $r = r_c$. The maximum tensile stress at the fracture tip (i.e., at $\alpha = 0$) due to the mod–Istress intensity factor can be presented as follows:

$$\sigma_{tip,y}|_{\alpha=0} = \frac{K_I}{\sqrt{2\pi r_c}}. \tag{2}$$

Furthermore, the stress induced by the stress intensity of hydraulic cracks projected on the interface surface of natural fracture can be presented as

$$\begin{cases} \sigma_{tip,\beta r} = \dfrac{K_I}{\sqrt{2\pi r_c}}\cos\dfrac{\beta}{2} - \dfrac{K_I}{\sqrt{2\pi r_c}}\dfrac{\sin\beta}{2}\sin\dfrac{3\beta}{2}\cos 2\beta + \dfrac{K_I}{\sqrt{2\pi r_c}}\dfrac{\sin\beta}{2}\cos\dfrac{3\beta}{2}\sin 2\beta \\[2mm] \sigma_{tip,\beta\beta} = \dfrac{K_I}{\sqrt{2\pi r_c}}\cos\dfrac{\beta}{2} + \dfrac{K_I}{\sqrt{2\pi r_c}}\dfrac{\sin\beta}{2}\sin\dfrac{3\beta}{2}\cos 2\beta - \dfrac{K_I}{\sqrt{2\pi r_c}}\dfrac{\sin\beta}{2}\cos\dfrac{3\beta}{2}\sin 2\beta \\[2mm] \tau_{tip,\beta} = \dfrac{K_I}{\sqrt{2\pi r_c}}\dfrac{\sin\beta}{2}\sin\dfrac{3\beta}{2}\sin 2\beta + \dfrac{K_I}{\sqrt{2\pi r_c}}\dfrac{\sin\beta}{2}\cos\dfrac{3\beta}{2}\cos 2\beta \end{cases} \tag{3}$$

where K_I is the stress intensity factor, MPa·m$^{1/2}$; and r and θ are the polar coordinates at the fracture tip, using units m and (°) respectively.

2.2. In Situ Horizontal Stress

The maximum stress induced by in situ horizontal stress can be presented as

$$\sigma_{remote,y}|_{\alpha=0} = -\sigma_h. \tag{4}$$

At the same time, the stresses projected on the interface from the remote in situ stresses σ_H and σ_h are

$$\begin{cases} \sigma_{remote,\beta r} = -\dfrac{\sigma_H+\sigma_h}{2} - \dfrac{\sigma_H-\sigma_h}{2}\cos 2\beta \\[2mm] \sigma_{remote,\beta\beta} = -\dfrac{\sigma_H+\sigma_h}{2} + \dfrac{\sigma_H-\sigma_h}{2}\cos 2\beta \\[2mm] \tau_{remote,\beta} = \dfrac{\sigma_H-\sigma_h}{2}\sin 2\beta \end{cases}. \tag{5}$$

2.3. Stress Interference between Hydraulic Fractures

With the aim of analyzing the fracture propagation behavior by use of the displacement discontinuity method (DDM), the crack was regarded as a discrete displacement unit along a segment with a finite length. We managed this segment as an inner boundary condition of this problem. This segment was divided into a number of small units so as to consider the displacement discontinuity on each element to be a constant. Hence, for each specific discretized unit, the analytic solution for the discrete displacement problem could be easily generated. As a result, the solution corresponding to one such problem with variable discrete displacement could then be produced on the basis of the principle of superposition on all units, individually.

Consider a simple line element in x–y coordinate system. It has constant displacement discontinuity. As illustrated in Figure 3, we assume that there are *N* number hydraulic fractures along with the wellbore for the former profile, with the length of the fractures being equal to L_N. Alternatively, there are *M* hydraulic fractures along with the wellbore for latter profile, with the length of all fractures being equal to L_M. The hydraulic fracture is discretized into *m* boundary units, and the *j*-th boundary unit of the *i*-th hydraulic fracture can be denoted as $D^{i,j}n$ and $D^{i,j}s$.
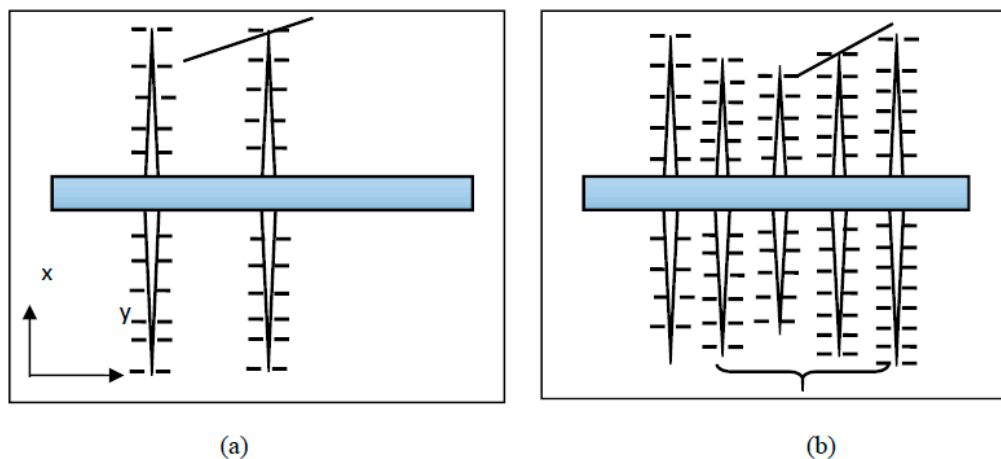

(a)　　　　　　　　　　　　　　　　　　　　　　(b)

Figure 3. The illustration of discretion of fractures: (**a**) multi-stage fracturing (**b**) multi-cluster fracturing.

2.3.1. Stress Boundary Condition

Network fracturing technology for clay formation contains sequential multi-stage hydraulic fracturing and simultaneous multi-stage hydraulic fracturing. Hydraulic fractures are induced individually and sequentially for the former (seen from Figure 1a), while hydraulic fractures are induced simultaneously for the latter (seen from Figure 1b). In terms of the former profile, the spacing of the adjacent two fractures is so large that the stress interference of the adjacent fractures should be considered, while the impacts of remote fractures can be neglected. Therefore, two adjacent fractures are considered for the former profile, namely, $N = 2$. In terms of the latter profile, the spacing of the adjacent two fractures is so small that the stress interference of all the fractures cannot be neglected. Therefore, all hydraulic fractures are considered for the former profile. The boundary conditions of arbitrary units are as follows:

$$\begin{cases} Multi-stage: \tau_s^{i,j} = 0, \sigma_s^{i,j} = -P_N^{i,j}, (i=1,2,...,N; j=1,2,...,m) \\ Multi-cluster: \tau_s^{i,j} = 0, \sigma_s^{i,j} = -P_N^{i,j}, (i=1,2,...,M; j=1,2,...,m) \end{cases} . \tag{6}$$

To consider the influence of fluid pressure inside the hydraulic fractures, the distribution of pressure profile inside each fracture can be presented based on the PKN (Perkins-Kem-Nordgren) model, namely

$$P_N(x,y) = P_o(1 - |x|/L)^{0.25}. \tag{7}$$

2.3.2. Mathematical Model of Stress Interference

On the foundation of the approach suggested by Olson et al. [14], the interference stress induced by the j-th boundary unit of the i-th hydraulic fracture, denoted as $D^{i,j}n$ and $D^{i,j}s$, at the arbitrary location (x,y) can be presented:

$$\begin{cases} \sigma_{inter,x}(x,y) = \sum_{i=1}^{k}\sum_{j=1}^{m} A_{xx}D_{i,jn} + \sum_{i=1}^{k}\sum_{j=1}^{m} A_{xy}D_{i,js} \\ \sigma_{inter,y}(x,y) = \sum_{i=1}^{k}\sum_{j=1}^{m} A_{yx}D_{i,jn} + \sum_{i=1}^{k}\sum_{j=1}^{m} A_{yy}D_{i,js} \quad , (k=N) \\ \tau_{inter,xy}(x,y) = \sum_{i=1}^{k}\sum_{j=1}^{m} A_{sx}D_{i,jn} + \sum_{i=1}^{k}\sum_{j=1}^{m} A_{sy}D_{i,js} \end{cases} \tag{8}$$

where A_{xx}, A_{xy}; A_{yx}, A_{yy}; and A_{sx}, A_{sy} are as follows:

$$\begin{aligned} A_{xx} &= 2G\left[2f_{xy} + \overline{y}f_{xyy}\right], A_{xy} = 2G\left[-f_{xx} + \overline{y}f_{yyy}\right] \\ A_{yx} &= 2G\left[-\overline{y}f_{xyy}\right], A_{yy} = 2G\left[f_{yy} - \overline{y}f_{yyy}\right] \\ A_{sx} &= 2G\left[2f_{yy} + \overline{y}f_{yyy}\right], A_{xy} = 2G\left[-\overline{y}f_{xyy}\right] \end{aligned} \tag{9}$$

$$f(x,y) = \frac{1}{4\pi(1-v)}\left[y\left(\arctan\frac{y}{x-a} - \arctan\frac{y}{x+a}\right) - (x-a)\ln\sqrt{(x-a)^2 + y^2} + (x+a)\ln\sqrt{(x+a)^2 + y^2}\right] \tag{10}$$

where, f_{xy}, f_{xx}, f_{xyy}, and f_{yyy} are, respectively, the second-order and third-order derivations of function $f(x,y)$ with respect to x and y.

When each boundary unit is selected, all of the boundary units can form a 2*M (former fracturing technology), or M*m (latter fracturing technology), order linear function system. Combined with boundary condition Equations (6) and (7), all of the displacement discontinuity $D^{i,j}n$ and $D^{i,j}s$ for all discretized boundary elements can be calculated. Finally, the stress interference for arbitrary location can also be calculated.

3. Mathematical Establishment of Propagation Behavior

The crossing behavior between a hydraulic crack and a pre-existing crack is quite complicated. Previous laboratory and field tests have demonstrated that some possible scenarios will exist when the hydraulic crack gradually approaches the natural crack and then directly crosses it (Figure 4). To clearly determine the mechanisms of these situations, this process can be divided into several steps, as follows.

(a)   (b)

Figure 4. The illustration of crossing between the hydraulic fracture and natural fracture: (**a**) crossing, and (**b**) arrested. The oval represents the hydraulic fracture, the thin, black line represents the natural fracture, and the bold, blue line represents the opening natural fracture.

When the tip of a hydraulic fracture approaches the natural cracks, there will be two possible events for the case of crossing behavior, namely, the hydraulic fracture crosses over the natural fracture directly (Figure 4a) or the hydraulic fracture is captured by the natural fracture. The natural fracture is opened and re-initiated at a certain position on the natural fracture according to a certain initiation angle (Figure 4b). In short, the main aspects of fracture propagation consist of the crossing behavior and initiation angle.

3.1. Natural Fracture Stress Analysis

Now we select the natural fracture stress unit to be analyzed, as shown in Figure 5. Shear-compression stress of natural fracture (σ_H, σ_h) is a comprehensive crustal stress, P_f is the net stress in the natural crack, the intersection angle between the natural crack and the maximum horizontal principal stress is θ, the fracture initiation angle over the natural fracture tip is α, and the natural crack half-length is b.
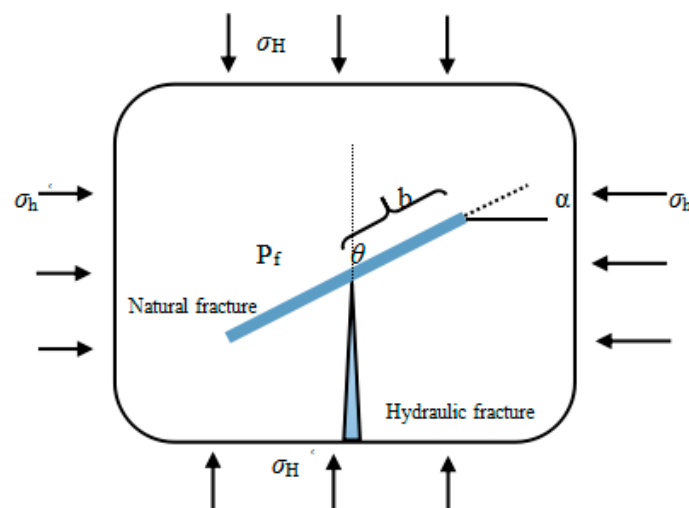

Figure 5. The illustration of stress on natural fracture unit.

Because the natural fracture surface suffers from compressive and shear stresses simultaneously, the natural fracture can incur shear and slip damage simultaneously, so the fracture propagation behavior can be simplified as I–II style brittle fracture of the composite fracture under the action of shear-compression.

According to interrelated theory about fracture mechanics, the I–II style stress intensity factors on the tip of crack can be respectively defined as [15]

$$\begin{cases} K_I = \sigma \sqrt{\pi b} \\ K_X = \tau \sqrt{\pi b} \end{cases} \tag{11}$$

In the above formula, σ and τ represent the shearing and cutting stresses over the natural fracture in MPa.

3.2. The Model of the Fracture Network Fracturing Initiation Angle

At present, the fracture initiation angle is calculated on the basis of the maximum circumferential stress criterion and the strain energy density factor theory. By using the maximum circumferential stress criterion, Gu et al. calculated the initiation angle when the hydraulic fracture penetrates the natural fracture [10]. Incorporating the maximum circumferential stress criterion, Cheng et al. calculated the initiation angle of the natural fracture [11]. On the basis of the strain energy density factor theory, Shao et al. established the initiation angle model by simultaneously considering the opening and shear slip modes [12]. In this paper, with the consideration of stress interference effects, we establish an initiation angle model using the maximum circumferential stress criterion and the strain energy density factor theory simultaneously.

Based on the previous analysis, the comprehensive stress in random point can be presented as follows:

$$\begin{cases} \sigma_H{}' = \sigma_H - \sigma_{inter,x}(x,y) \\ \sigma_h{}' = \sigma_h - \sigma_{inter,y}(x,y) \\ \tau_{xy} = \tau_{inter,xy}(x,y) \end{cases} \tag{12}$$

Combining the stress–strength theory and natural fracture tip's stress components, I–II type conforms with the compression shear effect, and the circumferential stress of the natural fracture tip in the polar coordinates can be expressed as [15]

$$\sigma_\alpha = \frac{1}{2\sqrt{\pi r}} \cos \frac{\alpha}{2} [K_I(1 + \cos \alpha) - 3K_{\prod} \sin \alpha] \tag{13}$$

When the fracture cracks again along the maximum circumferential stress, the circumferential stress of the fracture tip is limited to

$$\frac{\partial \sigma_\alpha}{\partial \alpha} = \frac{-3}{4\sqrt{2\pi r}} \cos \frac{\alpha}{2} [K_I \sin \alpha + K_{\prod}(3\cos \alpha - 1)] = 0 \tag{14}$$

According to the actual conditions, the initiation angle α_1 is as follows:

$$K_I \sin \alpha_1 + K_{\prod}(3\cos \alpha_1 - 1) = 0 \tag{15}$$

Combining with the strain energy density factor theory, G.C. Sih gave the strain energy density S near the fracture tip as follows:

$$\begin{aligned} S = \frac{1}{16\pi\mu}(1 + \cos \alpha)(\frac{3-v}{1+v} - \cos \alpha)K_I{}^2 + \frac{1}{8\pi\mu} \sin \alpha(2\cos \alpha + 1 - \frac{3-v}{1+v})K_I K_{\prod} \\ + \frac{1}{16\pi\mu}[(\frac{3-v}{1+v} + 1)(1 - \cos \alpha) + (1 + \cos \alpha)(3\cos \alpha - 1)] \end{aligned} \tag{16}$$

When the fracture cracks again along the minimum strain energy density, by taking a limiting process of the fracture tip's circumferential stress, we can find that initiation angle α_2 meets the following formula:

$$\frac{1}{2}K_I{}^2(3\sin\alpha_2\cos\alpha_2 - \sin\alpha_2) + K_I K_{\amalg}(3\cos 2\alpha_2 - \cos\alpha_2)$$
$$+\frac{1}{4}K_{\amalg}{}^2(-9\sin 2\alpha_2 + 2\sin\alpha_2) = 0 \tag{17}$$

By solving Equations (14) and (16), we can get the fracture initiation angle according to the different fracture theory and the different approaching angle.

4. The Calculation and Analysis of Fracture Initiation Angle

In this section, we calculate and analyze the model of the secondary initiation angle of the crack direction change by considering the fracture stress interference under the conditions of fracture network fracturing technique in a shale reservoir. The relevant influencing factors are analyzed, and the basic data are shown in Table 1.

Table 1. The basic data from the model analysis.

Maximum Horizontal Principal Stress σ_H (MPa)	Minimum Horizontal Principal Stress σ_h (MPa)	Poission's Ratio v	Young's Modulus E (MPa)	Natural Fracture Half Length b (m)
40	25	0.25	25,000	10

4.1. The Comparison of the Initiation Angle Calculation Model

To analyze the single fracture propagation behavior, Cheng et al. (2014) and Gu et al. (2010) derived the calculation method for the initiation angle based on the maximum circumferential stress crack criterion. Combining with the strain energy density factor theory, Shao et al. (2014) built a calculation model of fracture initiation angle. However, all of the above criteria were constructed on the basis of a single hydraulic fracture propagation situation, and ignore the influence of stress interference on the initiation angle when multiple fractures extend simultaneously. This paper proposes a new calculation model of initiation angle by considering the stress interference among all hydraulic fractures. Three hydraulic fractures are used in this paper, and some other parameters are shown in Table 1.

Figure 6 shows the relationship between the initiation angle α and the crack approaching angle. We can conclude from the Figure 6 that, due to the existence of stress interference from the hydraulic fractures, the initiation angle of the hydraulic fracture decreases. Using the different stress principle, the initiation angle has little distinction. When considering stress interference, initiation angles are significantly distinctive under low intersection angle conditions, while under high intersection angle conditions, initiation angles are approximately similar.
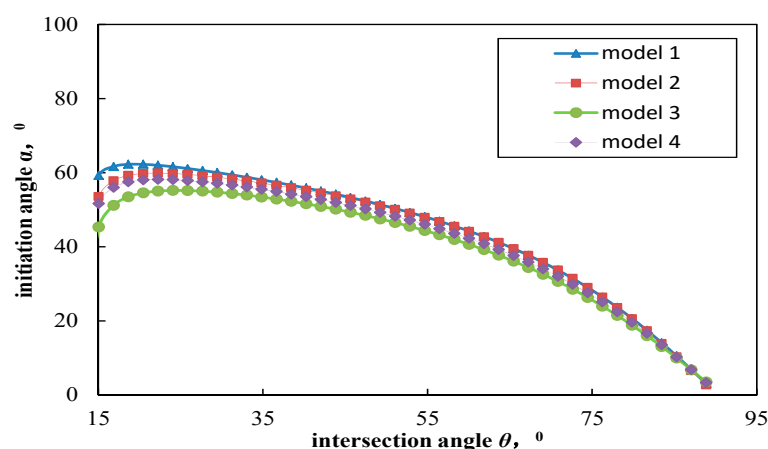

Figure 6. A comparison of different models. Model 1: single fracture and maximum circumferential stress crack criterion; model 2: single fracture and strain energy density; model 3: multiplied fracture and maximum circumferential stress crack; and model 4: multiplied fracture and strain energy density.

4.2. Analysis of Influencing Factors

Figure 7 shows the impact of the hydraulic fracture length on the initiation angle. We chose five different fracture lengths (L_f) of 40, 60, 80, 120, and 120 m. With an increase in the hydraulic fracture length, the initiation angle gradually decreased under a low intersection angle condition. With an increase in the intersection angle, the initiation angle basically did not change. These results demonstrate that although the induced stress will increase as the fracture length increases, the orientation of the natural fracture also offsets the overlapped stress.
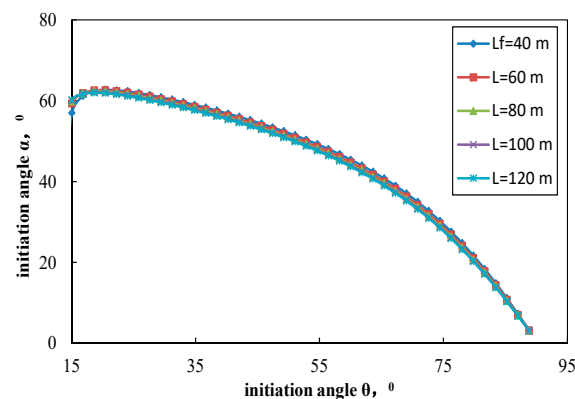
Figure 7. The impact of length of the fracture on the initiation angle.

Figure 8 shows the impact of the hydraulic fracture spacing on the initiation angle. We chose five different hydraulic fracture spacings (L) of 10, 20, 30, 40, and 50 m. As the crack spacing increased, the stress interference was weakened, induced stress at the tip of hydraulic fractures decreased, and the initiation angle first increased and then decreased. However, this does not mean that a small fracture spacing is favorable to forming a complex cracks structure.
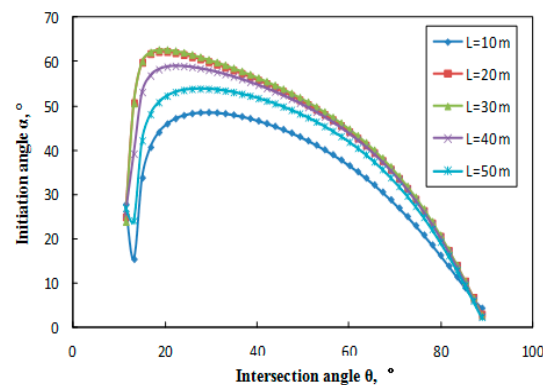

Figure 8. The impacts of distance of the fracture on the initiation angle.

Figures 9 and 10 show respectively that the relative position of the natural fracture and the natural fracture length have some impacts on the initiation angle. By an analysis of Figure 9, the initiation angles of the natural fracture around both ends that intersect with both the lateral fractures and the intermediate fractures were calculated respectively. We can conclude that the initiation angles of the same natural fracture around both ends are the same, and the initiation angle of the intermediate fracture is bigger than that of the lateral fracture. As we can see from Figure 10, the natural fracture length has little impact on the initiation angle in the case of a high approaching angle. However, under the condition of a low approaching angle, the smaller the natural fracture length is, the bigger the initiation angle is.
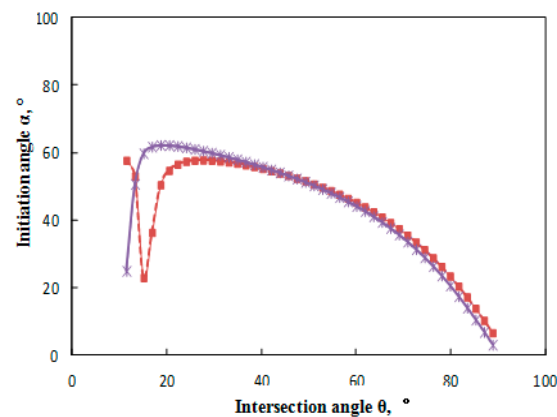
Figure 9. The impacts of relative position of the fracture on the initiation angle.
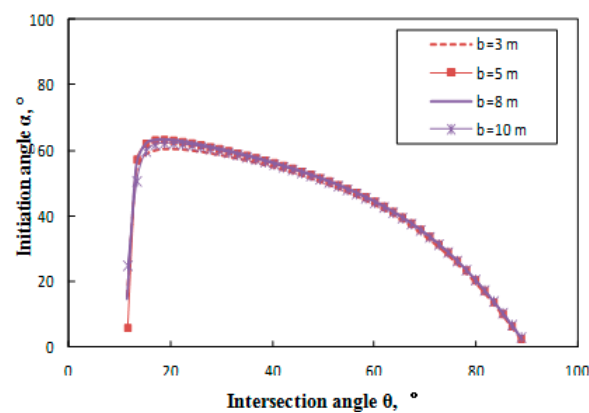

Figure 10. The impacts of net pressure on the initiation angle.

Figure 11 demonstrates that the net pressure on the hydraulic fractures play a role in the secondary initiation angle under the distinctive condition of single fracture and multiple fractures. In the case of a single fracture, as the net pressure among the hydraulic fracture increases, the initiation angle also increases. Under the condition of multiple fractures, because of the mutual interference among fractures, compressed stress formed on the natural fracture surface results in the net pressure on the hydraulic fracture causing the initiation angle to decrease. Meanwhile, in either case, under the condition of a low approaching angle, the net pressure among the hydraulic fracture has significant effects on the initiation angle, and as the net pressure increases, the initiation angle becomes bigger.
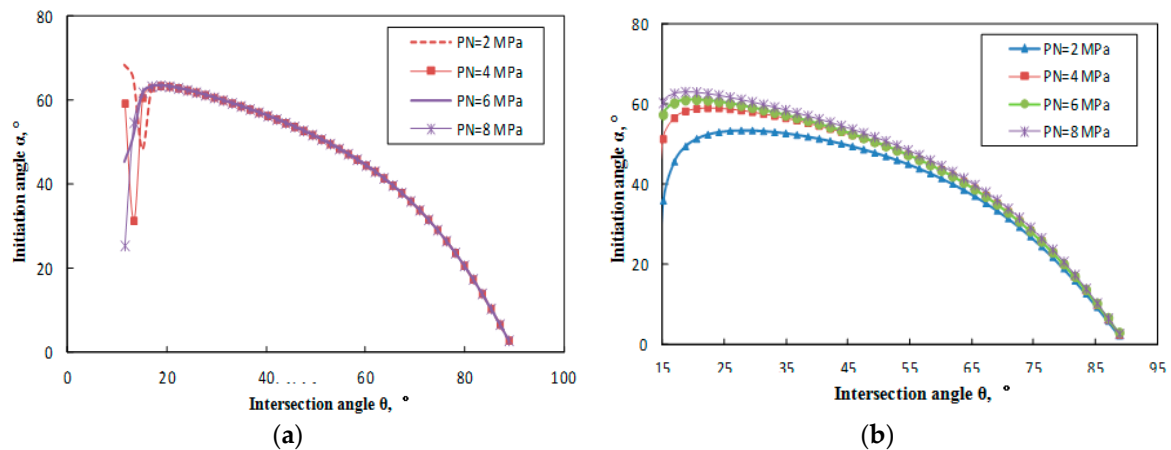

(a)

(b)

Figure 11. The impacts of net pressure on the initiation angle for (**a**) multiple fractures, and (**b**) a single fracture.

5. Conclusions

Based on the maximum circumferential stress criterion and the minimum strain energy density criterion respectively, a new secondary initiation angle of clay formation was established, with the consideration of the far-field crustal stress and stress interference among multiple-fractures.

Due to the existence of stress interference at the tip of fractures, the initiation angle of the hydraulic fractures decreases when the stress interference among fractures is considered. In terms of the different stress principle, the initiation angle has few distinctions. When considering stress interference, initiation angles are sensitive under a low intersection angle while the initiation angles are approximately the same under a high intersection angle condition.

The crack length, crack spacing, relative position of the natural fracture, and the net pressure inside the fractures have distinct influences on the initiation angle. Specifically, the length of the hydraulic fracture and natural fracture have little influence on the magnitude of the initiation angle. As the crack spacing increases, crack interference is reduced and thus, the initiation angle first increases and then decreases. Differing from single fracture propagation, owing to the stress interference among multiplied fractures, as the net pressure fractures increases, the initiation angle does not change significantly in the case of a high approaching angle. The initiation angle changes with the net pressure under the condition of low approaching angles, as the greater the net pressure is, the smaller the initiation angle is.

References

1. Jia, C.; Zheng, M.; Zhang, Y. Unconventional hydrocarbon resources in China and the prospect of exploration and development. *J. Pet. Explor. Dev.* **2012**, *39*, 129–136. [CrossRef]
2. Zhao, J. Conception, classification and resource potential of unconventional hydrocarbon. *J. Nat. Gas Geosci.* **2012**, *23*, 393–406.
3. Wu, Q.; Xu, Y.; Wang, X.; Wang, T.; Zhang, S. Volume fracturing technology of unconventional reservoirs: Connotation, optimization design and implementation. *J. Pet. Explor. Dev.* **2012**, *39*, 352–358. [CrossRef]
4. Zhao, J.; Li, Y.; Wang, S.; Zhang, L. Simulation of a complex fracture network influenced by natural fractures. *J. Nat. Gas Geosci.* **2014**, *34*, 68–73.
5. Daneshy, A.A. Hydraulic fracture propagation in the presence of planes of weakness. *Soc. Pet. Eng.* **1974**, *4852*, 8.
6. Blanton, T.L. An experimental study of interaction between hydraulically induced and pre-existing fractures. *Soc. Pet. Eng.* **1982**, *10847*, 13.
7. Palaniswamy, K.; Knauss, W.G. On the problem of crack extension in brittle solids under general loading. *J. Mech. Today* **1978**, *4*, 87–148.
8. Erdogan, F.; Sih, G.C. On the crack extension in plates under plane loading and transverse shear. *J. Basic Eng.* **1963**, *85*, 519–525. [CrossRef]
9. Sih, G.C. Some basic problems in fracture mechanics and new concepts. *Eng. Fract. Mech.* **1973**, *5*, 365–377. [CrossRef]
10. Gu, H.; Weng, X. *Criterion for Fractures Crossing Frictional Interfaces at Non-Orthogonal Angles*; American Rock Mechanics Association: Salt Lake City, UT, USA, 2010.
11. Cheng, Y.; Chang, X.; Sun, Y. Research on fracture network propagation pattern of shale reservoir based on fracture mechanics. *Nat. Gas Geosci.* **2014**, *25*, 603–611.

12. Shao, S.; Tian, S.; Li, G.; Sheng, M. Propagating orientation of hydraulic fractures in muddy shale formation. *Pet. Drill. Technol.* **2014**, *42*, 603–611.

13. Crouch, S.L.; Starfield, A.M. *Boundary Element Methods in Solid Mechanics*, 1st ed.; George Allen & Unwin Ltd.: London, UK, 1983.

14. Olson, J.E.; Arash, D.T. Modeling simultaneous growth of multiple hydraulic fractures and their interaction with natural fracture. In Proceedings of the SPE Hydraulic Fracturing Technology Conference, The Woodlands, TX, USA, 19–21 January 2009.

15. Rahman, M.K.; Hossain, M.M.; Rahman, S.S. An analytical method for mixed-mode propagation of pressurized fractures in remotely compressed rocks. *Int. J. Fract.* **2000**, *103*, 243–258. [CrossRef]